Supplementary Materials for:

Quaternary rainfall variability is governed by insolation in northern China and ice-sheet forcing in the South

Debo Zhao[1]*, Zhengyao Lu[2]*, Shiming Wan[1, 3, 4], Hai Cheng[5], Xuefa Shi[6], Anchun Li[1]

[1] Key Laboratory of Marine Geology and Environment, Institute of Oceanology, Chinese Academy of Sciences, Qingdao 266071, China.

[2] Department of Physical Geography and Ecosystem Science, Lund University, Sölvegatan 12, 22362, Lund, Sweden.

[3] Laboratory for Marine Geology, Qingdao National Laboratory for Marine Science and Technology, Qingdao 266061, China.

[4] CAS Center for Excellence in Quaternary Science and Global Change, Xi'an, 710061, China.

[5] Institute of Global Environmental Change, Xi'an Jiaotong University, Xi'an, 710054, China.

[6] Key Laboratory of Marine Sedimentology and Environmental Geology, First Institute of Oceanography, Ministry of Natural Resources, Qingdao, 266061, China.

* Corresponding Author: zhaodebo@qdio.ac.cn (D. Zhao), zhengyao.lu@nateko.lu.se (Z, Lu)

This PDF file includes:

Supplementary Discussion

Sediment provenance tracing

IODP Site U1429 has multiple potential sediment sources including the great rivers of East Asia (Yellow and Yangtze Rivers), as well as small mountainous rivers in nearby southern Kyushu of Japan, the Korean peninsula and the island of Taiwan (Fig. S1a).

The Yellow River in northern China has long been regarded as a typical large river influenced by intense catchment erosion. It is globally known for its very high sediment flux (~11 billion ton/yr, before 1980s) sourced mainly from the Chinese Loess Plateau (~90 % of sediments) in the middle reaches of the river [1,2]. After entering the sea, the fine-grained particles of these sediments have been transported to the Okinawa Trough by cross-shelf currents [3]. This has been tested repeatedly by sediment source tracing works using clay minerals, Sr-Nd-Pb isotopes and rare earth elements in past few years [4-7].

The nearby Kyushu island of Japan supplies 1.8 Mt of suspended sediments annually to East China Sea via the Chikugo River [1]. However, sediment source tracing works found the grain size population of Kyushu sediments deposited at U1429 is much coarser (30-63μm) than clay sized fractions (<2 μm) [4,8]. This is probably due to the short distance of sediment transport and plentiful rainfall on Kyushu, which facilitate the quick delivery of the primary products of land weathering and erosion to the study region [9]. In this study, our K/Al record is analyzed based on the clay-sized sediments. Thus we considered the effects of Kyushu sediments should be very minor.

The modern Yangtze River delivers 470 Mt of suspended sediments annually to the East China Sea [1]. However, most of the Yangtze River sediments are thought to accumulate off the river mouth and adjacent coastal area to the south, due to strong southward coastal current [10]; where only a small portion of fine-grained particles is transported offshore, and further to the middle and southern regions of the Okinawa Trough [11,12].

Rivers in the southern Korean Peninsula including the Seumjin and Nakdong, deliver about 10 Mt of suspended materials annually to the Tsushima Strait [1]. However, there is almost no sediment input in the study region from the Korean Peninsula [4-7]. This is probably due to the strong blocking effect of the Tsushima Warm Current and/or East Korean Warm Current and Korean Coastal Current, which transports sediments into the Japan Sea [13].

Taiwanese rivers collectively discharge about 200 Mt of sediments annually into the surrounding ocean [1]. However, more than half of them (~120 Mt) are delivered into the South China Sea and the Taiwan Strait [1]. Previous studies have indicated that Taiwan-derived sediments have only been transported to the southern [11,14] and middle Okinawa Trough via the Kuroshio Current [15].

The rare earth elements (REEs) have been widely applied as provenance tracers in East Asian marginal seas [5,16,17]. Here we compare UCC-normalized REE patterns of IODP Site U1429 clay-sized sediments with potential sources (Fig. S2a). It is obvious that samples of Site U1429 have similar REE patterns to the Yellow River sediments, and thus probably indicates their Yellow River sources. In view of the grain-size effect may regulate the REE composition, further the robust source tracing method with Nd isotope has been adopted. Nd isotopic composition of Site U1429 samples have been compared to the potential source end-members. The εNd vs. potential sediment source plot suggests similar Nd isotopic composition between clay-sized sediments at Site U1429 and Yellow River end-member, including Yellow River floodplain sediment samples, sediments from a sediment core since the last deglacial in the Yellow River month, and loess samples in Chinese Loess Plateau (Fig. S2b). As a result, based on the Nd isotope and REE source tracing results, we proposed that the clay-sized sediments at Site U1429 are dominantly supplied from Yellow River, which are mainly eroded from the Loess Plateau. Eolian dust contributes to the Yellow River sediment composition can be ignored, due to the extremely low dust supply with the dust column burdens only ranges from 0.21 to 0.28 g/m^2 in the observational sites of northern China [18].

Reconstruction of rainfall proxy in the Northern China

The single source of clay-sized sediments at Site U1429 provides the realizability to reconstruct the silicate weathering history of provenance area in northern China. It has been proposed that ~90% sediments in Yellow River are supplied from the Loess Plateau [19,20]. This can be proved by similar Nd isotopic composition between sediments in Yellow River and Loess Plateau [4]. Thus chemical weathering occurs mainly during the transport of sediments from Loess Plateau to Site U1429. It has been proposed that chemical weathering on sediments can hardly proceed after deposition in the ocean environment in the East Asian marginal seas [5,14]. As a result, chemical weathering of Site U1429 sediments should mainly occur on land, which shows strong response to rainfall and temperature conditions [21,22]. Hydraulic sorting effects on the mineral and further chemical composition have been eliminated due to the unitary grain size (<2 μm) extracted from the bulk samples [23].

The chemical weathering intensity of sediments can be deduced by a quantitative estimation of the chemical weathering of silicates, such as the calculated values of chemical index of alteration

(CIA) [24]. CIA is defined as $Al_2O_3/(Al_2O_3 + CaO^* + Na_2O + K_2O) \times 100$ (molar content; CaO* is the CaO content in the silicate fraction of the sample), which has long been used as a quantitative estimation of the chemical weathering intensity, based on the relative mobility of Na, K and Ca in aqueous fluids compared to immobile Al [5,24,25]. In addition, chemical weathering intensity can also be evaluated for mobilized elements (e.g., K) during incongruent weathering of silicates by comparing their concentration to that of a non-mobile element (e.g., Al) [26]. As a result, lower values of ratios of K/Al indicate more depletion of mobile elements in sediments and thus higher chemical alteration. Our CIA and K/Al proxies suggest consistent trend with dominant precession cycles (Fig. S3b and c).

By reducing the residence time of sediments, higher erosion rate can suppress weathering alteration [22]. Generally, higher physical erosion rate of Yellow River sediments largely depends on runoff, which is mainly regulated by enhanced rainfall in the drainage basin [27]. However, our decreased K/Al ratio (increased chemical weathering degree) corresponds to the high simulated rainfall amount (Fig. 2d and Fig. S3c), suggesting physical erosion is not a major control on chemical weathering in the Yellow River drainage basin.

The Yellow River basin has an arid to semi-arid continental climate, being more arid and cold in the upper and middle reaches, and more humid and temperate in the lower reaches. Our river sediment samples distribute from upper to lower reaches, and thus their K/Al ratios can show different responses to the distinct climate conditions, despite they were collected in a single season. Thus here we use them to establish a model covering variables including K/Al, rainfall and temperature based on the multiple statistical analyses. Because the high correlation between temperature and rainfall (Fig. S1d), the collinearity diagnosis was made on the standardized variables (variable $V_{K/Al}$, $V_{rainfall}$ and $V_{temperature}$ transform to $Z_{K/Al}$, $Z_{rainfall}$ and $Z_{temperature}$ respectively) firstly, to test if there was collinearity between these two independent variables. The variance inflation factor (VIF) is 6.322, which is large than 1, suggesting a collinearity problem (Table S1). Thus before linear regression, the dimensionality of the data is reduced with the Principal Component Analysis (PCA). Highly correlated independent variables can thus be transformed into mutually independent variables without linear relationship. Here, one component has been selected due to it can explain 95.875% of the variable variance (Tables S2 and S3). This transformed variable (Z1) can reflect most of the information of the original data. Then linear regression has been conducted on $Z_{K/Al}$ and Z1, to obtain a regression model covers K/Al ratio, temperature and rainfall. The p-value associated with the test statistic for transformed variable (Z1) is 0.002, which is less than 0.05. Thus we can conclude that the predictor variable Z1 is statistically significant (Table S4). Due to the p-value is larger than 0.05, the constant has been excluded. Then regression equation can be formed: $Z_{K/Al} = -0.606 \times Z1$.

Further, based on the following equations:

Standardized equation: $Z_m = (V_m - \text{average}_m) / SD_m$ (1)

Transform equation between transformed variable and independent variables: $Z1 = (Z_{score(rainfall)} \times Z_{rainfall} + Z_{score(temperature)} \times Z_{temperature}) / \sqrt{\lambda}$ (2)

The *m* is variables of K/Al, temperature and annual rainfall. Values of average and SD of K/Al, temperature and annual rainfall is 0.268 and 0.152, 11.240 and 2.858, 422.990 and 159.758, respectively. $Z_{score(rainfall)}$ and $Z_{score(temperature)}$ are all 0.979 (Table S3). The value of λ is 1.918 (Table S2).

As a result, we obtained the regression equation: $V_{K/Al} = -0.023 \times V_{temperature} - 0.00041 \times V_{rainfall} + 0.7$. This model can be used to predict the result of one variable (rainfall) given the two other variables (K/Al and temperature). The temperature used here was from [28]. Based on this regression model, the calculated mean annual rainfall during the last 400 ka ranges from ~470–717 mm (Fig. S3d). This is close to the modern annual rainfall (~562–648 mm) in the Yellow River middle to lower reaches [29], and our simulated annual rainfall (~407–854 mm) (daily rainfall multiply by 365 days) in northern China during the last 300 ka (Fig. 2d). Thus we considered our reconstructed quantitative rainfall variation is reliable.

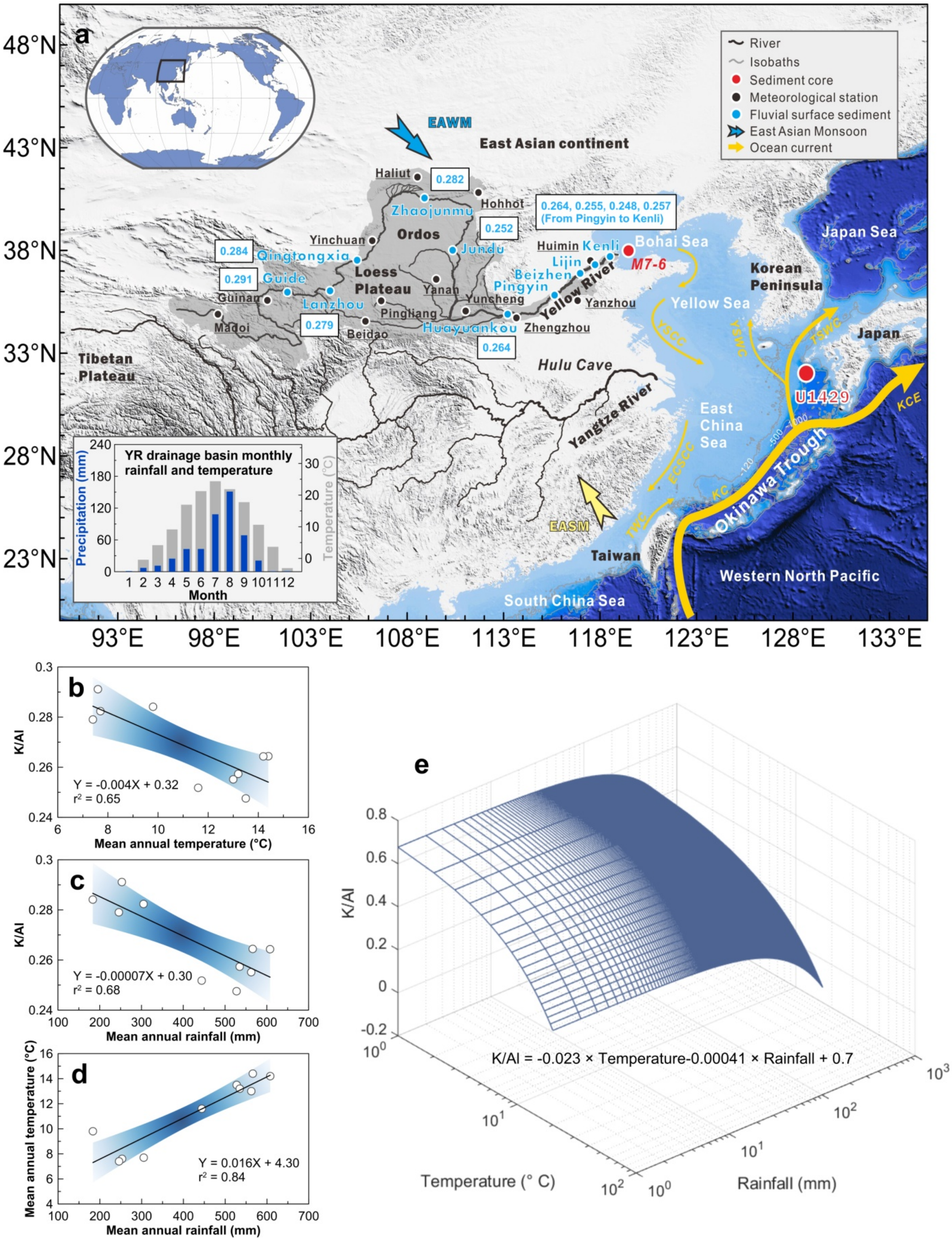

Supplementary Figure 1. Map showing locations of the study sites in East Asia and its marginal seas, as well as the relationship between chemical weathering proxy and climate. a Locations of IODP Site U1429 in the northern East China Sea, surface sediment samples and meteorological stations in the Yellow River drainage basin. Inserted global map shows the location of East Asia. Changes in precipitation and temperature for each month indicate that rainfall in the

Northern China is mainly contributed from the summer months. Precipitation and temperature data used here are from NOAA NCEI (https://www.ncei.noaa.gov/maps/global-summaries/). The ocean current system is changed from [3]. YSCC, Yellow Sea Coastal Current; YSWC, Yellow Sea Warm Current; TSWC, Tsushima Warm Current; ECSCC, East China Sea Coastal Current; KC, Kuroshio Current; KCE, Kuroshio Current Extension; TWC, Taiwan Warm Current. White numbers on grey isobaths show water depths. Blue numbers show K/Al ratios of Yellow River surface sediment samples. **b, c and d** Correlations among the chemical weathering proxy K/Al, mean annual temperature and rainfall in the Northern China. Meteorological data are from nearby meteorological stations from the China Meteorological Data Service Center. Black lines and blue shaded area are linear fits of meteorological data and the 95% confidence limits, respectively. **e** Plot of regression equation for K/Al, rainfall and temperature.

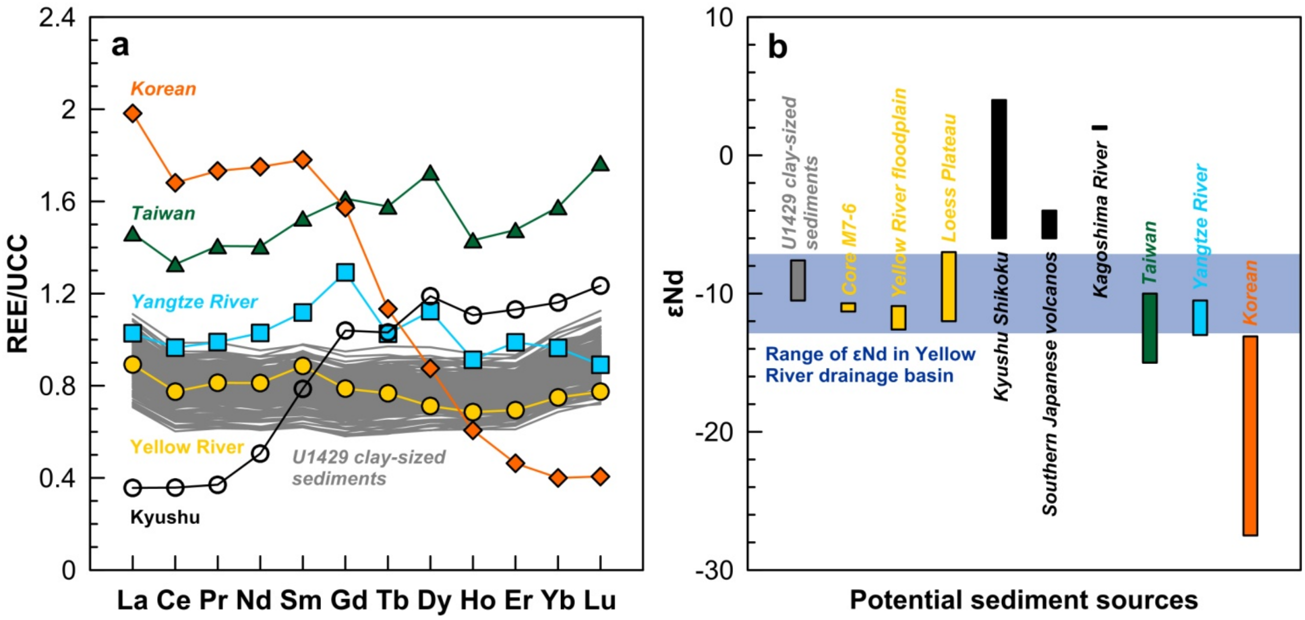

Supplementary Figure 2. Provenance analysis of clay-sized sediments at IODP Site U1429. a Comparison of UCC-normalized fractionation patterns of REE composition for sediments of U1429 (this study) and river sediments from Yellow River (<74 μm) [30], Yangtze River (<74 μm) [30], Taiwan rivers (<63 μm) [31], Korean rivers (<100 μm) [32] and Kyushu volcanic rocks [33]. **b** Comparison of Nd isotopic compositions between sediments from U1429 and potential source areas. Nd isotopic compositions from: U1429 clay-sized fraction [4], Yellow River [34-36], Yangtze River [34-36], Taiwan [37,38], Korean rivers [39], Loess Plateau [40-42], Kyushu Shikoku [43], Kagoshima River [4], and southern Japanese volcanos [43-45].

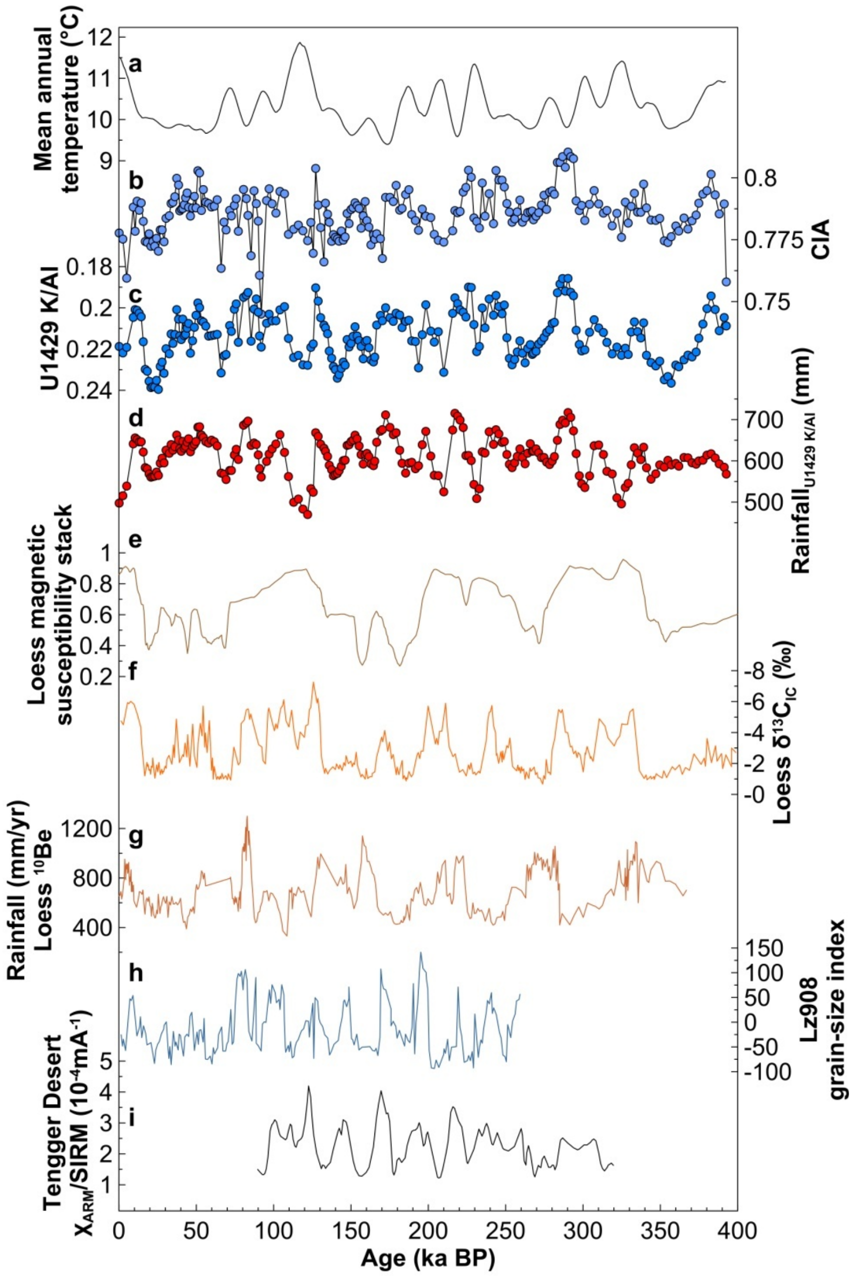

Supplementary Figure 3. Rainfall proxies in the Northern China. **a** Simulated Northern China mean annual temperature [28]. **b and c** CIA and K/Al of clay-sized sediments at Site U1429. **d** Reconstructed rainfall amount of northern China based on the weathering proxy of Site U1429. **e** Composite magnetic susceptibility record of loess-paleosol sequence from the Loess Plateau [46]. **f** $\delta^{13}C_{IC}$ record in the Loess Plateau [28,47]. **g** Loess ^{10}Be rainfall record [48]. **h** Northern China rainfall proxy at core Lz908 located onshore near the southern coast of the Bohai Sea [49]. **i** Northern China rainfall record of sediment borehole in Chahanchi Lake in Tengger Desert [50].

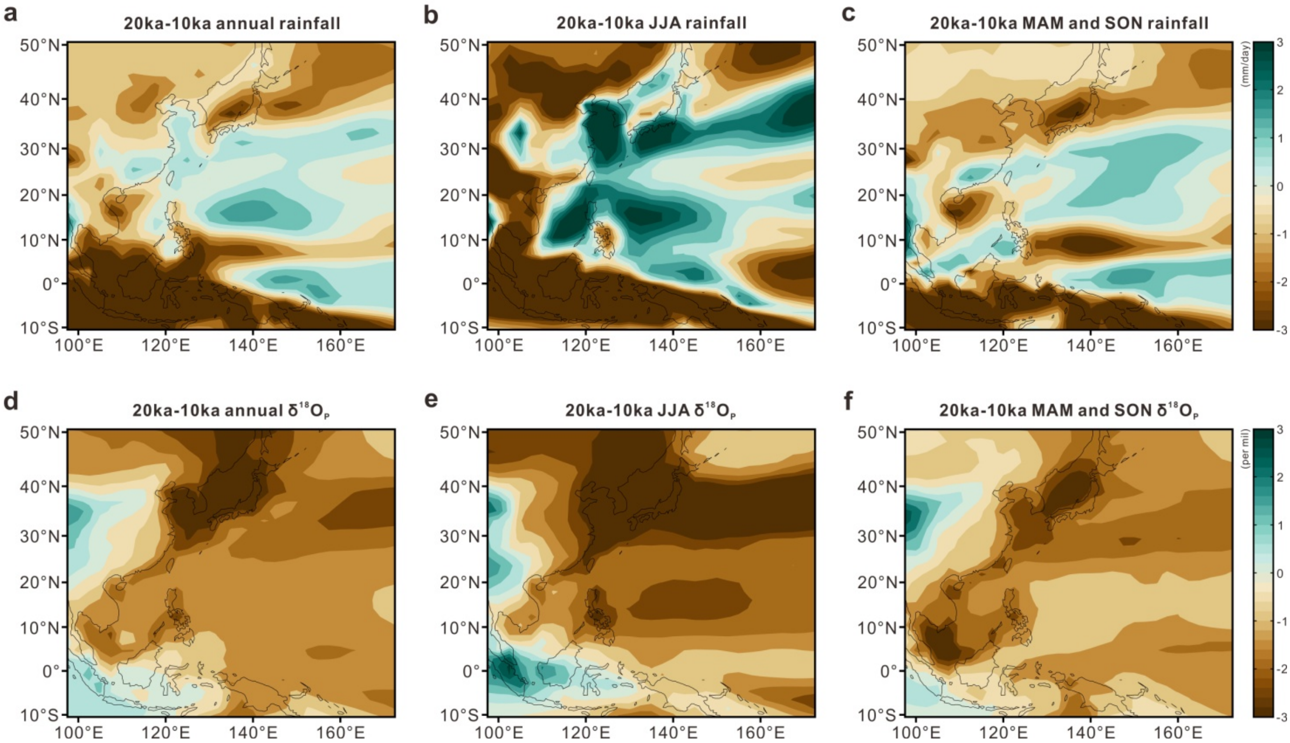

Supplementary Figure 4. Simulated differences of rainfall and water δ^{18}O between 20 and 10 ka in East-Southeast Asia. a–c annual, summer (JJA), spring (MAM) and autumn (SON) rainfall, respectively. **d–f** the same with a–c but for water δ^{18}O.

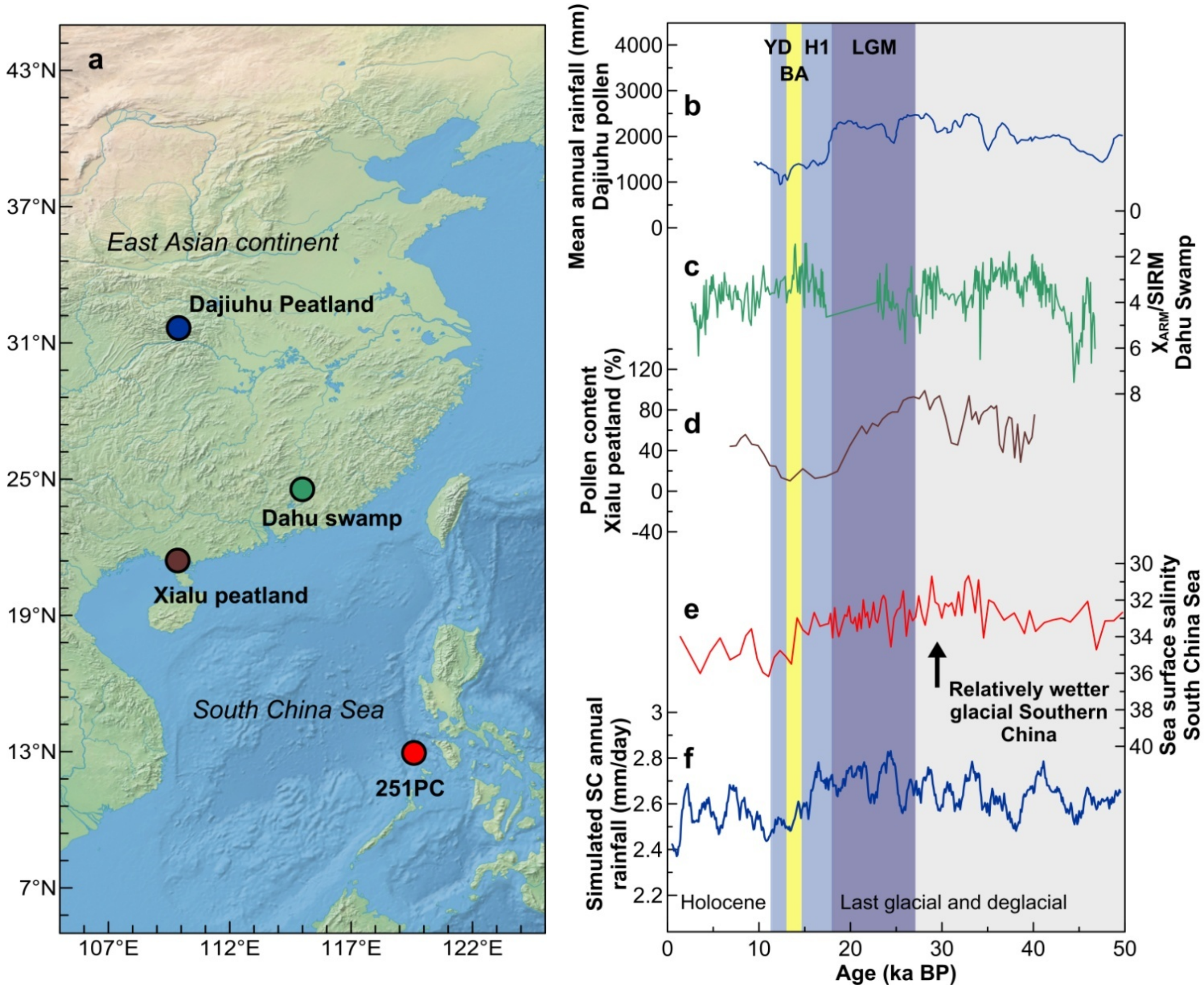

Supplementary Figure 5. Rainfall records in the southern China. a Rainfall records in southern China and South China Sea. **b** Dajiuhu pollen record [51]. **c** Dahu Swamp magnetic record [52]. **d** Xialu peatland pollen record [53]. **e** South China Sea sea surface salinity record [54]. **f** Simulated Southern China rainfall (this study), and the selected domain is shown in Figure 1b. All of these records suggest wetter southern China and South China Sea during glacial periods.

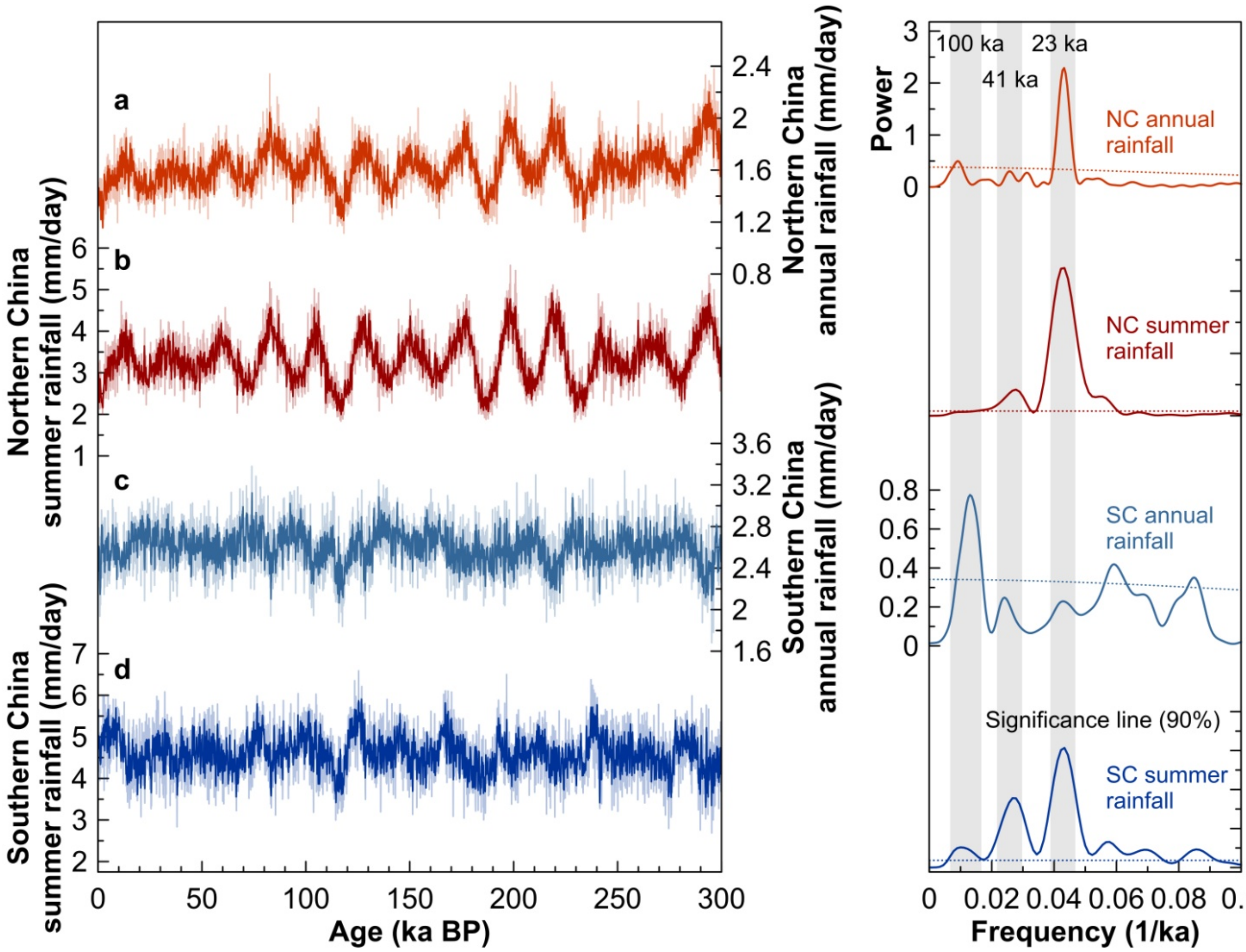

Supplementary Figure 6. Simulated annual and summer rainfall in China (left), as well as their corresponding spectral analysis results (right). a and b Northern China annual and summer rainfall, respectively. **c and d** Southern China annual and summer rainfall, respectively. The selected domains of Northern China (NC) and Southern China (SC) are shown in Figure 1b. Spectral analysis has been performed with PAST software [55]; the window function is rectangle. The gray vertical bars shown in the right panel mark the orbital periodicities.

Supplementary Table 1.

Supplementary Table 1. Coefficients in collinearity diagnosis for the independent variables.

Coefficients[a]								
Model		**Unstandardized Coefficients**		**Standardized Coefficient**	t	Sig.	**Collinearity Statistics**	
		B	Std.Error	Beta			Tolerance	VIF
1	(Constant)	-3.895E-16	.194		.000	1.000		
	Zscore(Temperature)	-.337	.515	-.337	-.654	.534	.158	6.322
	Zscore(Rainfall)	-.521	.515	-.521	-1.011	.346	.158	6.322

a. Dependent variable: Zscore (Weathering)

Supplementary Table 2.

Supplementary Table 2. Total variance explained in Principal Component Analysis.

Total Variance Explained						
Component	Initial Eigenvalues			Extraction Sum of Squared Loadings		
	Total	% of Variance	Cumulative %	Total	% of Variance	Cumulative %
1	1.918	95.875	95.875	1.918	95.875	95.875
2	.082	4.125	100.000			
Extraction Method: Principal Component Analysis						

Supplementary Table 3.

Supplementary Table 3. Component matrix in Principal Component Analysis.

Component Matrix[a]	
	Component
	1
Zscore(Temperature)	.979
Zscore(Rainfall)	.979
Extraction Method: Principal Component Analysis	
a. 1 component extracted	

Supplementary Table 4.

Supplementary Table 4. Coefficients in linear regression.

Coefficients[a]								
Model		**Unstandardized Coefficients**		**Standardized Coefficient**	t	Sig.	**Collinearity Statistics**	
		B	Std.Error	Beta			Tolerance	VIF
1	(Constant)	-3.600E-16	.182		.000	1.000		
	Z1	-.606	.139	-.840	-4.373	.002	1.000	1.000
a. Dependent variable: Zscore (Weathering)								

Supplementary References

1 Milliman, J. D. & Farnsworth, K. L. *River discharge to the coastal ocean: a global synthesis*. (Cambridge University Press, 2013).

2 Wang, S. et al. Reduced sediment transport in the Yellow River due to anthropogenic changes. *Nature Geoscience* **9**, 38–41 (2016).

3 Yuan, D., Zhu, J., Li, C. & Hu, D. Cross-shelf circulation in the Yellow and East China Seas indicated by MODIS satellite observations. *Journal of Marine Systems* **70**, 134–149 (2008).

4 Beny, F., Toucanne, S., Skonieczny, C., Bayon, G. & Ziegler, M. Geochemical provenance of sediments from the northern East China Sea document a gradual migration of the Asian Monsoon belt over the past 400,000 years. *Quaternary Science Reviews* **190**, 161–175 (2018).

5 Zhao, D. et al. Provenance, sea-level and monsoon climate controls on silicate weathering of Yellow River sediment in the northern Okinawa Trough during late last glaciation. *Palaeogeography Palaeoclimatology Palaeoecology* **490**, 227–239 (2018).

6 Zhao, D. et al. Asynchronous variation in the Quaternary East Asian winter monsoon associated with the tropical Pacific ENSO-like system. *Geophysical Research Letters* (2019).

7 Zhao, D. et al. Distinct control mechanism of fine-grained sediments from Yellow River and Kyushu supply in the northern Okinawa Trough since the last glacial. *Geochemistry Geophysics Geosystems* **18** (2017).

8 Zhao, D., Wan, S., Lu, Z., Zhai, L. & Li, A. Response of heterogeneous rainfall variability in East Asia to Hadley circulation reorganization during the late Quaternary. *Quaternary Science Reviews* **247** (2020).

9 Sidle, R. C. & Chigira, M. Landslides and debris flows strike Kyushu, Japan. *Eos, Transactions American Geophysical Union* **85**, 145–151 (2004).

10 Dong, J. et al. Holocene Climate Modulates Mud Supply, Transport, and Sedimentation on the East China Sea Shelf. *Journal of Geophysical Research: Earth Surface* **125**, e2020JF005731 (2020).

11 Diekmann, B. et al. Detrital sediment supply in the southern Okinawa Trough and its relation to sea-level and Kuroshio dynamics during the late Quaternary. *Marine Geology* **255**, 83–95 (2008).

12 Zheng, X. et al. ITCZ and ENSO pacing on East Asian winter monsoon variation during the Holocene: sedimentological evidence from the Okinawa Trough. *Journal of Geophysical Research: Oceans* **119**, 4410–4429 (2014).

13 Chun, J.-H. et al. Late Holocene distal mud deposits off the Nakdong delta, SE Korea: evidence for shore-parallel sediment transport in a current-dominated setting. *Geo-Marine Letters* **35**, 475–485 (2015).

14 Dou, Y. et al. Provenance weathering and erosion records in southern Okinawa Trough sediments since 28 ka: geochemical and Sr-Nd-Pb isotopic evidences. *Chemical Geology* **425**, 93–109 (2016).

15 Zheng, X. et al. Synchronicity of Kuroshio Current and climate system variability since the Last Glacial Maximum. *Earth and Planetary Science Letters* **452**, 247–257 (2016).

16 Dou, Y. et al. Provenance discrimination of siliciclastic sediments in the middle Okinawa Trough since 30 ka: constraints from rare earth element compositions. *Marine Geology* **275**, 212–220 (2010).

17 Um, I. K., Man, S. C., Lee, G. S. & Chang, T. S. Origin and depositional environment of fine-grained sediments since the last glacial maximum in the southeastern Yellow Sea: evidence from rare earth elements. *Geo-Marine Letters* **35**, 421–431 (2015).

18 Wang, X., Liu, J., Che, H., Ji, F. & Liu, J. Spatial and temporal evolution of natural and anthropogenic dust events over northern China. *Scientific Reports* **8**, 2141, (2018).

19 Ren, M. & Shi, Y. Sediment discharge of the Yellow River (China) and its effect on the sedimentation of the Bohai and the Yellow Sea. *Scientia Geographica Sinica* **6**, 785–810 (1986).

20 Yang, S., Jung, H. S. & Li, C. Two unique weathering regimes in the Changjiang and Huanghe drainage basins: geochemical evidence from river sediments. *Sedimentary Geology* **164**, 19–34 (2004).

21 Kump, L. R., Brantley, S. L. & Arthur, M. A. Chemical Weathering, Atmospheric CO2, and Climate. *Annual Review of Earth & Planetary Sciences* **28**, 611–667 (2000).

22 West, A. J. Thickness of the chemical weathering zone and implications for erosional and climatic drivers of weathering and for carbon-cycle feedbacks. *Geology* **40**, 811–814 (2012).

23 Guo, Y. et al. Revisiting the effects of hydrodynamic sorting and sedimentary recycling on chemical weathering indices. *Geochimica et Cosmochimica Acta* **227**, 48–63 (2018).

24 Nesbitt, Amp, H. W. & Young, G. M. Early proterozoic climates and plate motions inferred from major element chemistry of lutites. *Nature* **299**, 715–717 (1982).

25 Clift, P. D., Wan, S. & Blusztajn, J. Reconstructing chemical weathering, physical erosion and monsoon intensity since 25 Ma in the northern South China Sea: A review of competing proxies. *Earth-Science Reviews* **130**, 86–102 (2014).

26 Nesbitt, H. W. & Young, G. M. Formation and Diagenesis of Weathering Profiles. *Journal of Geology* **97**, 129–147 (1989).

27 Wang, W., Yin, S., Gao, G., Papalexiou, S. M. & Wang, Z. Increasing trends in rainfall erosivity in the Yellow River basin from 1971 to 2020. *Journal of Hydrology* **610**, 127851 (2022).

28 Sun, Y. et al. Diverse manifestations of the mid-Pleistocene climate transition. *Nature Communications* **10**, 352 (2019).

29 Chang, J., Wei, J., Wang, Y., Yuan, M. & Guo, J. Precipitation and runoff variations in the Yellow River Basin of China. *Journal of Hydroinformatics* **19**, 138–155 (2016).

30 Yang, S. Y., Jung, H. S., Man, S. C. & Li, C. X. The rare earth element compositions of the Changjiang (Yangtze) and Huanghe (Yellow) river sediments. *Earth & Planetary Science Letters* **201**, 407–419 (2002).

31 Li, C. S. *et al.* Rare earth elements in fine-grained sediments of major rivers from the high-standing island of Taiwan. *Journal of Asian Earth Sciences* **69**, 39–47 (2013).

32 Lee, S. G., Kim, J. K., Yang, D. Y. & Kim, J. Y. Rare earth element geochemistry and Nd isotope composition of stream sediments, south Han River drainage basin, Korea. *Quaternary International* **s 176–177**, 121–134 (2008).

33 Shinjo, R., Woodhead, J. D. & Hergt, J. M. Geochemical variation within the northern Ryukyu Arc: magma source compositions and geodynamic implications. *Contributions to Mineralogy & Petrology* **140**, 263–282 (2000).

34 Goldstein, S., O'nions, R. & Hamilton, P. A Sm-Nd isotopic study of atmospheric dusts and particulates from major river systems. *Earth and planetary Science letters* **70**, 221–236 (1984).

35 Yang, S. Y., Jiang, S. Y. & Ling, H. F. Sr-Nd isotopic composition of Changjiang River sediments:implications for tracing sediment sources. *Science in China* **50**, 1556–1565 (2007).

36 Bayon, G. et al. Rare earth elements and neodymium isotopes in world river sediments revisited. *Geochimica et Cosmochimica Acta* **170**, 17–38 (2015).

37 Chen, C.-H., Jahn, B.-M., Lee, T., Chen, C.-H. & Cornichet, J. Sm-Nd isotopic geochemistry of sediments from Taiwan and implications for the tectonic evolution of southeast China. *Chemical Geology* **88**, 317–332 (1990).

38 John, B., Zhou, X. & Li, J. Formation and tectonic evolution of southeastern China and Taiwan: isotopic and geochemical constraints. *Tectonophysics* **183**, 145–160 (1990).

39 Lan, C.-Y., Lee, T., Zhou, X.-H. & Kwon, S.-T. Nd isotopic study of Precambrian basement of South Korea: Evidence for Early Archean crust? *Geology* **23**, 249–252 (1995).

40 Chen, J. et al. Nd and Sr isotopic characteristics of Chinese deserts: Implications for the provenances of Asian dust. *Geochimica et Cosmochimica Acta* **71**, 3904–3914 (2007).

41 Hu, B. et al. Provenance and climate change inferred from Sr-Nd-Pb isotopes of late Quaternary sediments in the Huanghe (Yellow River) Delta, China. *Quaternary Research* **78**, 561–571 (2012).

42 Sun, J. Nd and Sr isotopic variations in Chinese eolian deposits during the past 8 Ma: Implications for provenance change. *Earth and Planetary Science Letters* **240**, 454–466 (2005).

43 Mahoney, J. B. Nd and Sr isotopic signatures of fine-grained clastic sediments: A case study of western Pacific marginal basins. *Sedimentary Geology* **182**, 183–199 (2005).

44 Ishizaka, K. & Carlson, R. Nd-Sr systematics of the Setouchi volcanic rocks, southwest Japan: a clue to the origin of orogenic andesite. *Earth and Planetary Science Letters* **64**, 327–340 (1983).

45 Chen, C.-H., DePaolo, D. J., Nakada, S. & Shieh, Y.-N. Relationship between eruption volume and neodymium isotopic composition at Unzen volcano. *Nature* **362**, 831 (1993).

46 Sun, Y. et al. East Asian monsoon variability over the last seven glacial cycles recorded by a loess sequence from the northwestern Chinese Loess Plateau. *Geochemistry Geophysics Geosystems* **7**, 97–112 (2006).

47 Sun, Y. et al. Astronomical and glacial forcing of East Asian summer monsoon variability. *Quaternary Science Reviews* **115**, 132–142 (2015).

48 Beck, J. W. et al. A 550,000-year record of East Asian monsoon rainfall from ^{10}Be in loess. *Science* **360**, 877 (2018).

49 Yi, L. et al. Late Quaternary linkage of sedimentary records to three astronomical rhythms and the Asian monsoon, inferred from a coastal borehole in the south Bohai Sea, China. *Palaeogeography, Palaeoclimatology, Palaeoecology* **329–330**, 101–117, (2012).

50 Liu, C. et al. Eccentricity forcing of East Asian monsoonal systems over the past 3 million years. *Proceedings of the National Academy of Sciences* **118**, e2107055118 (2021).

51 Xiao, J., Xiao, X., Zhang, M., Shang, Z. & Chen, Y. Late Pleistocene montane vegetation and climate history from the Dajiuhu Basin in the western Hubei Province of Central China. *Review of Palaeobotany and Palynology* **222**, 22–32 (2015).

52 Wei, Z. et al. Late Quaternary East Asian Summer Monsoon Variability Deduced From Lacustrine Mineral Magnetic Records of Dahu Swamp, Southern China. *Paleoceanography and Paleoclimatology* **35**, e2019PA003796 (2020).

53 Xue, J., Zhong, W., Xie, L. & Unkel, I. Vegetation responses to the last glacial and early Holocene environmental changes in the northern Leizhou Peninsula, south China. *Quaternary Research* **84**, 223–231 (2015).

54 Zhou, Q. et al. Planktic foraminiferal $\delta^{18}O$ values indicate precipitation variability in the southeastern South China Sea over the last 175 ka BP. *Quaternary Science Reviews* **253**, 106745 (2021).

55 Hammer, Y., Harper, D. A. & Ryan, P. D. PAST: Paleontological statistics software package for education and data analysis. *Palaeontologia Electronica* **4**, 1–9 (2001).